

# Spectroscopy and Coherence of an Excited-State Transition in $\text{Tm}^{3+}:\text{YAlO}_3$ at Telecommunication Wavelength

Luozen Li,<sup>1,2,3,\*</sup> Akshay Babu Karyath,<sup>1,2,3,\*</sup> Mohsen Falamarzi Askarani,<sup>4,†</sup>  
Maria Gieysztor,<sup>4,5</sup> Hridya Meppully Sasidharan,<sup>4,‡</sup> Joshua A. Slater,<sup>4,§</sup>  
Sara Marzban,<sup>4,¶</sup> Nir Alfasi,<sup>4,\*\*</sup> Patrick Remy,<sup>6</sup> and Wolfgang Tittel<sup>1,2,3,††</sup>

<sup>1</sup>*Department of Applied Physics, University of Geneva, 1211 Geneva, Switzerland*

<sup>2</sup>*Constructor University Bremen, 28759 Bremen, Germany*

<sup>3</sup>*Constructor Institute of Technology, 8200, Schaffhausen, Switzerland*

<sup>4</sup>*QuTech, Delft Technical University, 2628 CJ Delft, Netherlands*

<sup>5</sup>*Institute of Physics, Faculty of Physics, Astronomy and Informatics, Nicolaus Copernicus University, Torun, Poland*

<sup>6</sup>*SIMH Consulting, Rue de Genève 18, 1225 Chêne-Bourg, Switzerland*

(Dated: November 10, 2025)

We characterize the spectroscopic and coherence properties of the 1451.37 nm excited-state zero-phonon line (ZPL) between the  $^3\text{F}_4$  and the  $^3\text{H}_4$  manifolds of a thulium-doped yttrium aluminum perovskite ( $\text{Tm}:\text{YAlO}_3$ ) crystal at temperatures around 1.5 K. We measure the absorption spectrum between the  $^3\text{H}_6 - ^3\text{F}_4$  and  $^3\text{F}_4 - ^3\text{H}_4$  manifolds, the inhomogeneous broadening of the  $^3\text{F}_4 - ^3\text{H}_4$  (excited-state) ZPL, and the lifetimes of the higher-lying and lower-lying excited states. We also investigate spectral hole-burning spectra with varying magnetic fields, which provides insight into hyperfine and superhyperfine interactions. Using again spectral holes but also optical free induction decays (FIDs), we assess optical coherence times, finding a maximum of 1.1  $\mu\text{s}$  when a 2T magnetic field is applied. Our results—the first to demonstrate coherence of an excited-state transition in a rare-earth crystal—suggest the possibility of exploiting such transitions for quantum technology.

*Introduction:* Starting with the development of protocols that enable the storage and faithful recall of quantum states of light 20 years ago [1–3], trivalent rare-earth ions doped into cryogenically cooled inorganic crystals have played an increasingly important role in the development of quantum technology [4]. Today, ensemble-based quantum memories have reached a level of performance that allows early demonstrations of quantum repeater infrastructure [5–10], and individual ions are being explored as single-photon sources [11, 12] and as qubits that allow quantum information processing [13–15]. At the heart of these applications is an important fundamental property – highly coherent transitions between electronic and spin levels with coherence times that can exceed milliseconds [16–19] and hours [20], respectively.

Surprisingly, while transitions between different (long-lived) excited states play an important role in solid-state lasers, e.g. the Nd-YAG laser [21], optical coherence at cryogenic temperatures of a few Kelvin has so far only been investigated for transitions starting at an electronic ground state. However, the long excited-state lifetimes that characterize the 4f levels of rare-earth ions allow, in principle, similarly long coherence times for excited-state transitions. In addition to being of fundamental interest, this would extend the use of rare-earth crystals to new wavelengths and novel applications. Here we investigate spectroscopic properties and optical coherence of the  $^3\text{F}_4$  to  $^3\text{H}_4$  excited-state transition in  $\text{Tm}:\text{YAlO}_3$ .

Several properties make  $\text{Tm}:\text{YAlO}_3$  a particularly interesting material to study. First, the transitions between its  $^3\text{F}_4$  and the  $^3\text{H}_4$  electronic manifolds comprise a so-called zero-phonon line (ZPL), i.e. the transition

between their lowest Stark levels (or crystal field levels) is allowed (see Fig. 1a for a simplified level scheme that shows the ZPL between Y1 and X1). Note that only ZPLs can be coherent and hence potentially useful for quantum technology. But be aware that the existence of a sharp ZPL for a given rare-earth-ion transition between two such manifolds cannot be taken for granted. To the best of our knowledge, so far only a few Tm-doped crystals, including  $\text{Tm}:\text{YAlO}_3$ , have been identified to feature an excited-state ZPL.

Second, the wavelength of the  $^3\text{F}_4$  to  $^3\text{H}_4$  ZPL is around 1450 nm, where transmission loss in standard optical fiber is almost as small as in the telcom C-band, 0.25 dB/km and 0.2 dB/km, respectively. This makes  $\text{Tm}:\text{YAlO}_3$  a promising alternative to erbium-doped crystals, which feature a ground-state transition at around 1532 nm that has been exploited both for single-photon sources and quantum memory for light [22–24].

And third, also shown in Fig. 1a,  $\text{Tm}:\text{YAlO}_3$  features three ZPLs—two ground-state transitions and one excited-state transition—that are arranged in a ring. This promises the development and implementation of novel protocols that require more than a single line, e.g. the creation of entangled photon pairs using two cascading transitions (transitions X1 - Y1 and Y1 - Z1 in Fig.1a) as originally proposed in [25], and quantum computing using one transition for optical state read-out (e.g. transition Z1 - X1) and another transition (e.g. transition Z1 - Y1) for dipole-blockade-based controlled 2-qubit gates, similar to the case of trapped ions [26].

$\text{Tm}:\text{YAlO}_3$  has previously been investigated for lasers at around 800 nm and 1800 nm wavelength [27], and

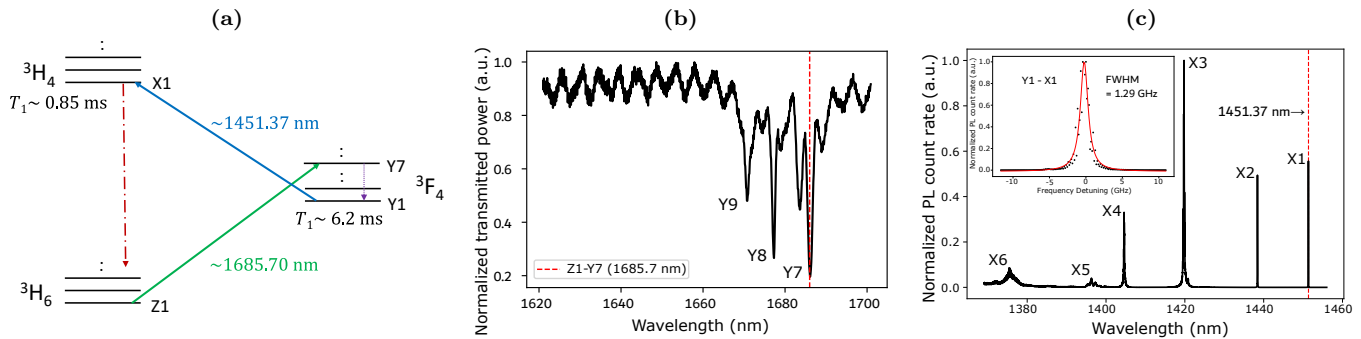


**FIG. 1:** (a) Energy levels of relevant transitions of  $\text{Tm}^{3+}$  in  $\text{YAlO}_3$ . (b) Transmission spectrum measured using a broadband LED, demonstrating absorption on Z1 to  ${}^3\text{F}_4$  transitions. (c) Photoluminescence (PL) rate at  $\sim 800\text{nm}$  as a function of wavelength of a laser exciting the Y1 to  ${}^3\text{H}_4$  transitions. The inset shows a zoom-in of the Y1 to X1 ZPL. The crystal field levels of the upper states are identified in panels b) and c).

excited-state absorption lines have been measured at room temperature [28]. But to the best of our knowledge, our investigation is the first to study an excited-state transition of a rare-earth crystal at cryogenic temperatures, where coherence properties can be assessed.

Our paper is organized as follows. First, we measure the absorption spectrum between the  ${}^3\text{H}_6$  and  ${}^3\text{F}_4$  manifolds, and we describe how we populate the Y1 level. We then extend the absorption measurements to transitions between the  ${}^3\text{F}_4$  and  ${}^3\text{H}_4$  manifolds, and we measure the inhomogeneous broadening of the ZPL at  $1451.37\text{ nm}$  as well as the lifetimes of the Y1 and X1 levels. Furthermore, we characterize spectral holes and free-induction decays as a function of the magnetic field, which allows us to assess the homogeneous linewidth of the  $1451.37\text{ nm}$  transition and its inverse, the coherence time. Finally, we probe the hyperfine structure and superhyperfine interaction by investigating magnetic field-dependent spectral hole splitting. To round off the paper, we discuss the next steps towards applications of  $\text{Tm}:\text{YAlO}_3$  in quantum information processing.

*Experimental Details:*  $\text{YAlO}_3$  features an orthorhombic unit cell with lattice constants  $a=5.179\text{ \AA}$ ,  $b=5.329\text{ \AA}$ ,  $c=7.370\text{ \AA}$  (Pbnm space group).  $\text{Tm}^{3+}$  substitutes  $\text{Y}^{3+}$  ions in sites with low point-group symmetry  $C_{1h}$  [29]. Measurements are carried out using a  $12.0\text{ mm} \times 2.2\text{ mm} \times 2.0\text{ mm}$  large  $0.1\%$  crystal (measured along the crystal axes (a, b, c)) (from Scientific Material Corp.). The crystal is glued to a customized Cu stage and further secured and thermalized by a Cu lid with spring-tensioned screws. It is cooled to around  $1.5\text{ K}$  using a pulse-tube cooler supplemented by an adiabatic demagnetization stage. A superconducting solenoid allows one to apply an approximately homogeneous magnetic field between  $0$  and  $2\text{ T}$  along the b-axis of the crystal.

The laser light is sent through the crystal along the a-axis using a single-mode (SM) pigtailed ferrule and a

gradient-index (GRIN) lens. The ferrule is attached to an attocube nanopositioner, which allows adjusting the distance between the ferrule and the GRIN lens to collimate the laser beam to a diameter of around  $0.3\text{ mm}$ . Behind the crystal, a mirror reflects the light back through the crystal and into the fiber. A tunable continuous-wave (CW) laser emitting at around  $1680\text{ nm}$  wavelength (Topica DL pro) is used for optical pumping, and another CW laser (Santec TSL-550) drives the excited-state transition at around  $1450\text{ nm}$  wavelength. One fiber-based acousto-optic modulator (AOM) per laser allows creating short pulses, and a phase modulator (PM) is used to modify the spectrum of the  $\sim 1450\text{ nm}$  laser light.

Depending on the experiment, we can choose between different detectors. To detect photoluminescence at  $795\text{ nm}$  wavelength caused by atomic decay from the  ${}^3\text{H}_4$  to the  ${}^3\text{H}_6$  manifold, a single-photon counting module (SPCM) based on a silicon-avalanche photodiode is used (from Perkin Elmer). In this case, we also employ free-space spectral filters (a low-pass filter composed of multiple EO2-coated mirrors and a DMSP950 dichroic mirror, all from Thorlabs) that reject light at  $1680\text{ nm}$  and  $1450\text{ nm}$ . For spectral hole burning measurements, the  $1450\text{ nm}$  laser light is directed to an InGaAs photoreceiver with  $10\text{ MHz}$  bandwidth (New Focus 2053). Finally, to characterize free induction decays (FIDs), a higher-bandwidth photoreceiver (New Focus 1811) with a rise and fall time of  $3\text{ ns}$  is used. It is preceded by a gating AOM that blocks irrelevant pulses. For a schematic of the optical setup, see the supplemental material.

*Optical pumping :* At  $1.5\text{ Kelvin}$ , the  $\text{Tm}^{3+}$  ions occupy the lowest crystal field level Z1 of the  ${}^3\text{H}_6$  ground-state multiplet. Since we are interested in the Y1 to X1 transition between the  ${}^3\text{F}_4$  and the  ${}^3\text{H}_4$  manifolds, our first goal is to pump atomic population from Z1 to Y1. As we can see in Figure 1a, there are two different approaches to addressing this challenge. First, we can pump ions

directly from the  ${}^3\text{H}_6$  Z1 (ground) state into the  ${}^3\text{F}_4$  manifold. Since intra-manifold relaxation between crystal field levels takes place on the nanosecond time scale [30], it is possible to excite ions into any  ${}^3\text{F}_4$  level, from where they then rapidly decay into Z1. This approach to pumping is promising since it allows one to interact continuously with an empty upper atomic level. In addition, one can choose the strongest absorption line. The second possibility is to pump ions from the ground state into the  ${}^3\text{H}_4$  manifold. A fraction of these ions will decay spontaneously into the  ${}^3\text{F}_4$  manifold (possibly through the  ${}^3\text{H}_5$  level, not shown in Fig. 1a) and eventually populate Y1. (The other fraction will decay back to  ${}^3\text{H}_6$ .) In the following, we have chosen the first approach due to its superior efficiency. A detailed discussion of the second approach, including measurement results, can be found in the supplemental material.

*Absorption spectra:* We study the absorption lines between Z1 and the  ${}^3\text{F}_4$  manifold by measuring the wavelength-dependent transmission of a broadband LED (DL-BZ1 from Denselight Semiconductors) using an optical spectrum analyzer (Anritsu MS9710C). Figure 1b shows several dips of transmitted power of around 1.5 to 3 nm width between 1620 nm and 1700 nm wavelength, the most relevant excited crystal field levels are indicated [31]. These transitions are highly polarization-dependent. After optimization using a fiber-optic polarization controller, we find that the Z1 to Y7 transition at 1685.7 nm features the strongest absorption. It is used in the following to populate the Y1 level.

Next, we measure the absorption spectrum of the Y1 to  ${}^3\text{H}_4$  transitions. After populating Y1 using the 1686 nm laser, we expose the crystal to laser light whose wavelength we scan between 1370 nm and 1456 nm in steps of 0.01 nm. The detection of photoluminescence (PL) at around 800 nm indicates resonances and, at the same time, allows optimizing the laser polarization and the initial pumping step. Our measurement results are shown in Fig. 1c. In particular, we find a well isolated line at 1451.37 nm, which, according to literature, is the ZPL between Y1 and X1 [29]. A subsequent laser scan around this wavelength with improved resolution of 0.001 nm reveals a linewidth of 1.29 GHz. This is much narrower than any of the ground-state transitions shown in Fig. 1b. We furthermore measure an optical depth of up to 1.12, which we expect to increase with optimized pumping (see the supplemental material).

Small variations of these measurements also allow establishing the radiative lifetimes of the Y1 and the X1 levels. For the former, we monitor the time-resolved decay of the optical depth of the Y1 to X1 transition after switching off the 1686 nm laser. For the latter, we analyze the decay of the 800 nm PL rate after pulsed excitation of the X1 level. We find lifetimes of 6.21 and 0.85 ms, respectively. See the supplemental material for details.

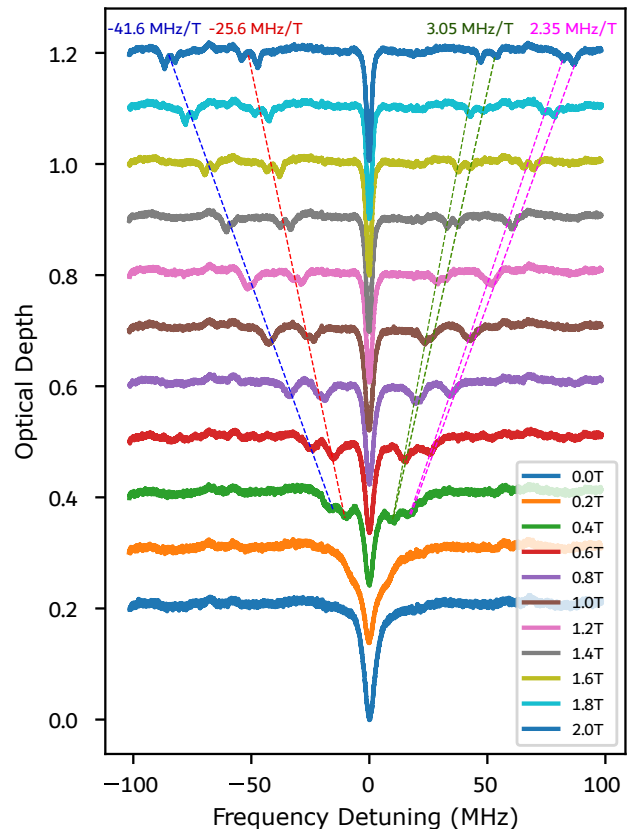


**FIG. 2:** Spectral hole burning spectra under varying magnetic fields. Traces measured with different fields are offset by an amount that is proportional to the field.

*Spectral Hole Burning:* To assess the magnetic field-dependent energy-level structure of the thulium ions as a consequence of the enhanced nuclear Zeeman effect [32], and to bound the coherence time of the Y1 to X1 excited state transition, we perform a series of spectral hole burning experiments. After populating Y1, we expose the Tm ions during a *burn time* of 300  $\mu\text{s}$  to narrow-bandwidth 1451 nm laser light. After waiting during a 10  $\mu\text{sec}$  long *wait time*, we scan the 1451 nm laser over a 200 MHz wide spectral interval that is centered on the burn frequency and we monitor the transmitted optical power. Figure 2 shows the resulting hole-burning spectra for magnetic fields between 0 and 2T, consisting of a central hole and two clusters of side holes on either side. We find that the width of the central hole decreases with increasing magnetic field, that the center of each cluster of side holes shifts linearly at rates of  $\pm 25.6$  MHz/T and  $\pm 41.6$  MHz/T away from the center, and that the two holes within each cluster also split as a function of the field. We also note the absence of anti-holes.

To explain the origin of these clusters (the splitting of the two holes within each cluster is discussed later), we take into account that thulium has a nuclear spin  $I =$

1/2, and that the hyperfine coupling between the nuclear spin and the electronic states splits each crystal field level into a pair of hyperfine levels [32]. As we further illustrate in the supplemental material, narrow-bandwidth optical pumping therefore drives four different transitions within the ensemble of inhomogeneously broadened thulium ions – one between each combination of a ground state and an excited state. This results in decreased absorption—a central hole and four side holes (becoming clusters due to additional level splitting)—at five different frequencies. Note that the sum of the burn and wait time is sufficiently small compared to the lifetime of the two magnetic X1 levels to exclude significant decay of atoms from X1 back into Y1 (in addition, the branching ratio for this pathway is rather small, and most decay leads back to the ground state). This explains the absence of anti-holes.

Next, we perform time-resolved spectral hole burning. We find that the two “inner” clusters (with splitting rate of  $\pm 25.6$  MHz/T) decay on a scale comparable to the radiative lifetime of X1 (0.85 ms). As explained in the supplemental material, this suggests that these clusters are caused by, and their detuning with respect to the central hole identifies, the splitting of the two hyperfine levels within the Y1 doublet. The other pairs of clusters, with splitting rate of  $\pm 41.6$  MHz/T, decay with a much longer lifetime, comparable to that of the central hole. We conjecture that they are caused by the splitting of the two hyperfine levels within the X1 doublet.

We now focus on the splitting between the two holes within each cluster. A linear fit results for the two inner clusters in a rate of 3.05 MHz/T and for the two outer clusters in a slightly smaller rate of 2.35 MHz/T. We attribute this additional splitting to superhyperfine coupling to the nuclear spin of lattice ions, most likely  $\text{Al}^{3+}$ , which splits each of the four hyperfine levels into two. Interestingly, only the side holes further split, while the central hole is unaffected. As described in the supplemental material, this can be explained if we assume that only lattice-spin conserving transitions are allowed. The splitting rate of the holes belonging to a specific cluster is then given by the difference between the superhyperfine splittings of the upper and lower hyperfine levels of the X1 and Y1 manifolds, respectively.

In addition to providing insight into hyperfine and superhyperfine interactions, the hole-burning spectra—i.e. the width of the central holes—also allow one to derive an upper bound for the homogeneous linewidth  $\gamma_{\text{hom}}$  and hence a lower bound for the optical coherence time  $T_2 = 1/(\pi\gamma_{\text{hom}})$  of the excited-state transition. Indeed, one can show that  $\gamma_{\text{hole}} = \gamma_{\text{hom}} \left(1 + \sqrt{1 + \chi^2 T_1 T_2}\right) + \gamma_{\text{laser}}$  [33]. Here,  $\gamma_{\text{hole}}$  is the full-width-at-half-maximum (FWHM) of the hole,  $\chi$  is the on-resonance Rabi frequency,  $T_1$  is the longitudinal relaxation time, and  $\gamma_{\text{laser}}$  describes the linewidth of the laser used for hole burning – around 200 kHz according to manufacturer specifica-

tions.

When the power of the burn pulse is sufficiently small (and  $\chi^2 T_1 \approx 0$ ), this equation can be simplified to  $\gamma_{\text{hole}} \approx 2\gamma_{\text{hom}} + \gamma_{\text{laser}}$ , and we find

$$T_2 = 2/[\pi(\gamma_{\text{hole}} - \gamma_{\text{laser}})]. \quad (1)$$

Figure 3 shows coherence times for different magnetic fields calculated using Eq. 1. Note that these results only represent lower bounds for  $T_2$  since narrower holes (and hence longer coherence times) may have been obtained using a more stable laser and less pump power. Furthermore, spectral diffusion that leads to an increased hole width as a function of waiting time is not accounted for. The FWHM of the narrowest spectral hole we measured is  $\gamma_{\text{hole}} = 746.10\text{kHz}$  (for  $B=2$  T and  $T=1.3$  K), corresponding to  $\gamma_{\text{hom}}=273$  kHz and  $T_2 = 1.17$   $\mu\text{sec}$  (see the supplemental material).

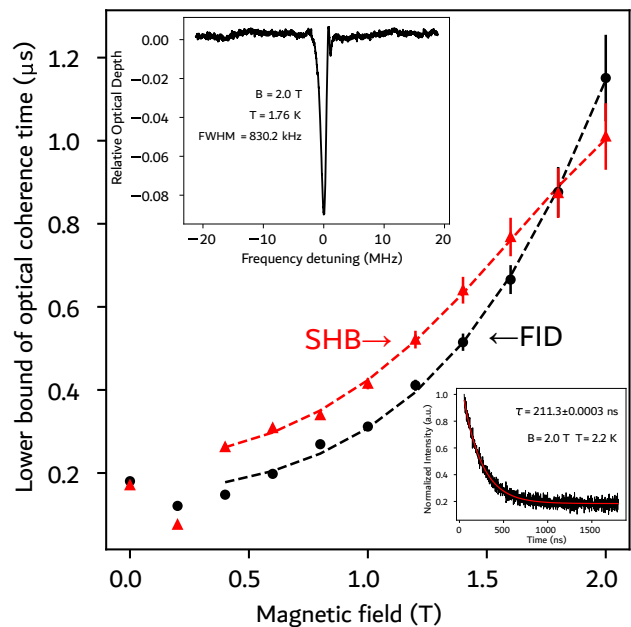


**FIG. 3:** Coherence times for different magnetic fields obtained by means of spectral hole burning (red triangles) and free induction decay (black dots). The insets show two measurement examples. Temperatures are 1.75 K and 2.22 K, respectively, explaining the slight difference between the results. The dashed lines are fits based on a spectral diffusion model. Error bars are calculated considering a laser linewidth uncertainty of  $\pm 50$  kHz.

*Free induction decay:* Another way to assess the optical coherence time is via the free induction decay (FID) [34]. In this case, ions are excited using a pulsed laser (pulse duration of 10  $\mu\text{s}$ ) with a bandwidth that is smaller than the homogeneous linewidth of the transition to be studied. The thereby created atomic polarization gives rise

to the emission of light, which decreases exponentially at the end of the laser pulse due to atomic dephasing.

As shown in the supplemental material,  $\tau_{\text{FID}} = 1/[2\pi(2\gamma_{\text{hom}} + \gamma_{\text{laser}})]$ , where  $\tau_{\text{FID}}$  is the 1/e decay of the intensity of the FID signal and  $\gamma_{\text{laser}} = (200 \pm 50)$  kHz. After solving for  $\gamma_{\text{hom}}$ , this leads to

$$T_2 = 1/(\pi\gamma_{\text{hom}}) = \frac{4}{1/\tau_{\text{FID}} - 2\pi\gamma_{\text{laser}}}. \quad (2)$$

The 2nd inset of Fig. 3 shows the FID intensity decay for  $B = 2$  T. An exponential fit results in  $\tau_{\text{FID}} = 211.3$  ns and in turn in  $T_2 = 1.15$   $\mu$ s. This and the values obtained for other magnetic fields are depicted in the main part of the same figure, along with the results for  $T_2$  obtained through spectral hole burning. Again, the calculated values constitute lower bounds, as the laser linewidth may exceed the homogeneous linewidth of the ions.

Both types of measurement show that the optical coherence time increases in our observation range ( $B \leq 2$  T) monotonously with increasing magnetic field. This suggests that decoherence is caused by flip-flops between the nuclear spins of neighboring lattice ions, most likely  $\text{Al}^{3+}$ ; the impact of phonon-driven spin flips, which leads to a decrease of  $T_2$  with increasing magnetic field, is insignificant [35, 36]. As shown in Figure 3, we fit our data using the optical decoherence model proposed in [37], finding indeed that spin-flips can be ignored. See the supplemental material for more information.

*Conclusion:* We have investigated an excited-state transition in  $\text{Tm}^{3+}:\text{YAIO}_3$  at cryogenic temperatures under varying magnetic fields, observing for the first time coherence of such a transition in any rare-earth ion doped crystal. In addition, we found a rich side-hole structure by means of spectral hole burning, providing insight into hyperfine and superhyperfine interactions.

To improve the optical coherence time, several avenues can be pursued. First, spin flips and flip-flops are suppressed at lower temperatures, and a longer optical coherence time can thus be expected by further cooling the crystal. Second, the magnetic field can be increased up to a point where spin flips become the primary limitation. And third, changing both the magnitude and the direction of the magnetic field may lead to spectrally stable optical clock transitions, which have been reported before for other rare-earth crystals [38, 39], including for Tm-doped crystals [40]. Finally, we note that one can easily change the concentration (and hence average distance) between Tm ions involved in the excited-state transition by changing the initial pumping step from Z1 to Y1. This enables control of instantaneous spectral diffusion, i.e. decoherence caused by the interactions between neighboring Tm ions upon excitation [41].

Overall, our results demonstrate the potential of excited-state transitions in REI-doped crystals for applications in quantum information processing. In particular, they open the path to true single-photon sources and

quantum memory within the telecom E band at 1450 nm – an alternative to erbium and potentially enabling the creation of quantum networks coexisting with classical communication at 1550 nm over the same fiber infrastructure [42].

## ACKNOWLEDGEMENTS

The authors thank Charles Thiel, Rufus Cone and their team for early input to these studies, and Javier Carrasco Ávila, Archi Gupta and Deeksha Gupta for discussions. We acknowledge funding through the Netherlands Organization for Scientific Research, the European Union’s Horizon 2020 Research and Innovation Program under Grant Agreement No. 820445 and Project Name Quantum Internet Alliance, and the Swiss State Secretariat for Education, Research and Innovation (SERI) under Contract Number UeM019-3.

\* These authors contributed equally to this work.

† Now at Xanadu Quantum Technologies Inc., Toronto, Ontario, M5G 2C8, Canada

‡ Current address unknown.

§ Now at Q\*Bird BV, 2628 XJ, Delft, The Netherlands.

¶ Now at PiCard Systems BV, 6525EC Nijmegen, The Netherlands

\*\* Now at Quantum Machines, Tel Aviv, Israel

†† Corresponding author: wolfgang.tittel@unige.ch

- [1] B. Kraus, W. Tittel, N. Gisin, M. Nilsson, S. Kröll, and J. I. Cirac, Quantum memory for nonstationary light fields based on controlled reversible inhomogeneous broadening, *Physical Review A—Atomic, Molecular, and Optical Physics* **73**, 020302 (2006).
- [2] A. L. Alexander, J. J. Longdell, M. J. Sellars, and N. B. Manson, Photon echoes produced by switching electric fields, *Physical review letters* **96**, 043602 (2006).
- [3] M. Nilsson and S. Kröll, Solid state quantum memory using complete absorption and re-emission of photons by tailored and externally controlled inhomogeneous absorption profiles, *Optics communications* **247**, 393 (2005).
- [4] W. Tittel, M. Afzelius, A. Kinos, L. Rippe, and A. Walther, Quantum networks using rare-earth ions, *Quantum Science and Technology* **10**, 033002 (2025).
- [5] N. Sangouard, C. Simon, H. De Riedmatten, and N. Gisin, Quantum repeaters based on atomic ensembles and linear optics, *Reviews of Modern Physics* **83**, 33 (2011).
- [6] N. Sinclair, E. Saglamyurek, H. Mallahzadeh, J. A. Slater, M. George, R. Ricken, M. Hedges, D. Oblak, C. Simon, W. Sohler, and W. Tittel, Spectral multiplexing for scalable quantum photonics using an atomic frequency comb quantum memory and feed-forward control, *Phys. Rev. Lett.* **113**, 053603 (2014).
- [7] X. Liu, J. Hu, Z.-F. Li, X. Li, P.-Y. Li, P.-J. Liang, Z.-Q. Zhou, C.-F. Li, and G.-C. Guo, Heralded entanglement distribution between two absorptive quantum memories, *Nature* **594**, 41 (2021).

- [8] D. Lago-Rivera, S. Grandi, J. Rakonjac, A. Seri, and H. de Riedmatten, Telecom-heralded entanglement between multimode solid-state quantum memories, *Nature* **594**, 37 (2021).
- [9] A. Ortu, A. Holzäpfel, J. Etesse, and M. Afzelius, Storage of photonic time-bin qubits for up to 20 ms in a rare-earth doped crystal, *npj Quantum Information* **8**, 29 (2022).
- [10] T.-X. Zhu, C. Zhang, Z.-W. Ou, X. Liu, P.-J. Liang, X.-M. Hu, Y.-F. Huang, Z.-Q. Zhou, C.-F. Li, and G.-C. Guo, A metropolitan-scale multiplexed quantum repeater with bell nonlocality, arXiv **2508.17940** (2025).
- [11] A. M. Dibos, M. Raha, C. M. Phenicie, and J. D. Thompson, Atomic source of single photons in the telecom band, *Phys. Rev. Lett.* **120**, 243601 (2018).
- [12] T. Zhong, J. M. Kindem, J. G. Bartholomew, J. Rochman, I. Craiciu, V. Verma, S. W. Nam, F. Marsili, M. D. Shaw, A. D. Beyer, and A. Faraon, Optically addressing single rare-earth ions in a nanophotonic cavity, *Phys. Rev. Lett.* **121**, 183603 (2018).
- [13] M. Raha, S. Chen, C. M. Phenicie, S. Ourari, A. M. Dibos, and J. D. Thompson, Optical quantum nondemolition measurement of a single rare earth ion qubit, *Nature Communications* **11**, 1605 (2020).
- [14] J. M. Kindem, A. Ruskuc, J. G. Bartholomew, J. Rochman, Y. Q. Huan, and A. Faraon, Coherent control and single-shot readout of a rare-earth ion embedded in a nanophotonic cavity, *Nature* **580**, 201 (2020).
- [15] A. Gritsch, A. Ulanowski, J. Pforr, and A. Reiserer, Optical single-shot readout of spin qubits in silicon, *Nature Communications* **16**, 64 (2025).
- [16] R. W. Equall, Y. Sun, R. L. Cone, and R. M. MacFarlane, Ultraslow optical dephasing in  $\text{Eu}^{3+}:\text{Y}_2\text{SiO}_5$ , *Phys. Rev. Lett.* **72**, 2179 (1994).
- [17] T. Böttger, C. Thiel, R. Cone, and Y. Sun, Effects of magnetic field orientation on optical decoherence in  $\text{Er}^{3+}:\text{Y}_2\text{SiO}_5$ , *Physical Review B—Condensed Matter and Materials Physics* **79**, 115104 (2009).
- [18] S. Welinski, A. Tiranov, M. Businger, A. Ferrier, M. Afzelius, and P. Goldner, Coherence time extension by large-scale optical spin polarization in a rare-earth doped crystal, *Phys. Rev. X* **10**, 031060 (2020).
- [19] M. F. Askarani, A. Das, J. H. Davidson, G. C. Amaral, N. Sinclair, J. A. Slater, S. Marzban, C. W. Thiel, R. L. Cone, D. Oblak, *et al.*, Long-lived solid-state optical memory for high-rate quantum repeaters, *Physical review letters* **127**, 220502 (2021).
- [20] M. Zhong, M. P. Hedges, R. L. Ahlefeldt, J. G. Bartholomew, S. E. Beavan, S. M. Wittig, J. J. Longdell, and M. J. Sellars, Optically addressable nuclear spins in a solid with a six-hour coherence time, *Nature* **517**, 177 (2015).
- [21] J. Geusic, H. Marcos, and L. Van Uitert, Laser oscillations in nd-doped yttrium aluminum, yttrium gallium and gadolinium garnets, *Applied Physics Letters* **4**, 182 (1964).
- [22] Y. Yu, D. Oser, G. Da Prato, E. Urbinati, J. C. Ávila, Y. Zhang, P. Remy, S. Marzban, S. Gröblacher, and W. Tittel, Frequency tunable, cavity-enhanced single erbium quantum emitter in the telecom band, *Physical review letters* **131**, 170801 (2023).
- [23] E. Saglamyurek, N. Sinclair, J. Jin, J. A. Slater, D. Oblak, F. Bussières, M. George, R. Ricken, W. Sohler, and W. Tittel, Broadband waveguide quantum memory for entangled photons, *Nature* **469**, 512 (2011).
- [24] E. Miyazono, T. Zhong, I. Craiciu, J. M. Kindem, and A. Faraon, Coupling of erbium dopants to yttrium orthosilicate photonic crystal cavities for on-chip optical quantum memories, *Applied Physics Letters* **108** (2016).
- [25] J. D. Franson, Bell inequality for position and time, *Physical review letters* **62**, 2205 (1989).
- [26] A. H. Myerson, D. J. Szwerc, S. C. Webster, D. T. C. Allcock, M. J. Curtis, G. Imreh, J. A. Sherman, D. N. Stacey, A. M. Steane, and D. M. Lucas, High-fidelity readout of trapped-ion qubits, *Phys. Rev. Lett.* **100**, 200502 (2008).
- [27] J. Körner, T. Lühder, J. Reiter, I. Uschmann, H. Marschner, V. Jambunathan, A. Lucianetti, T. Mücke, J. Hein, and M. C. Kaluza, Spectroscopic investigations of thulium doped YAG and YAP crystals between 77 k and 300 k for short-wavelength infrared lasers, *Journal of Luminescence* **202**, 427 (2018).
- [28] L. Guillemot, P. Loiko, J.-L. Doualan, A. Braud, and P. Camy, Excited-state absorption in thulium-doped materials in the near-infrared, *Optics Express* **30**, 31669 (2022).
- [29] J. O'hare and V. Donlan, Crystal-field determination for trivalent thulium in yttrium orthoaluminate, *Physical Review B* **14**, 3732 (1976).
- [30] C. W. Thiel, T. Böttger, and R. Cone, Rare-earth-doped materials for applications in quantum information storage and signal processing, *Journal of luminescence* **131**, 353 (2011).
- [31] V. Antonov, P. Arsenev, K. Bienert, and A. Potemkin, Spectral properties of rare-earth ions in  $\text{YAlO}_3$  crystals, *physica status solidi (a)* **19**, 289 (1973).
- [32] N. Sinclair, D. Oblak, E. Saglamyurek, R. L. Cone, C. W. Thiel, and W. Tittel, Optical coherence and energy-level properties of a  $\text{Tm}^{3+}$ -doped  $\text{LiNbO}_3$  waveguide at subkelvin temperatures, *Physical Review B* **103**, 134105 (2021).
- [33] H. de Vries and D. A. Wiersma, Photophysical and photochemical molecular hole burning theory, *The Journal of Chemical Physics* **72**, 1851 (1980).
- [34] R. G. Brewer and R. Shoemaker, Optical free induction decay, *Physical Review A* **6**, 2001 (1972).
- [35] Y. Bai and R. Kachru, Spin-fluctuation-induced optical spectral diffusion in  $\text{Pr}^{3+}:\text{YAlO}_3$ , *Physical Review A* **44**, R6990 (1991).
- [36] R. Yano, M. Mitsunaga, and N. Uesugi, Stimulated-photon-echo spectroscopy. i. spectral diffusion in  $\text{Eu}^{3+}:\text{YAlO}_3$ , *Physical Review B* **45**, 12752 (1992).
- [37] T. Böttger, C. Thiel, Y. Sun, and R. Cone, Optical decoherence and spectral diffusion at  $1.5 \mu\text{m}$  in  $\text{Er}^{3+}:\text{Y}_2\text{SiO}_5$  versus magnetic field, temperature, and  $\text{Er}^{3+}$  concentration, *Physical Review B—Condensed Matter and Materials Physics* **73**, 075101 (2006).
- [38] A. Ortu, A. Tiranov, S. Welinski, F. Fröwis, N. Gisin, A. Ferrier, P. Goldner, and M. Afzelius, Simultaneous coherence enhancement of optical and microwave transitions in solid-state electronic spins, *Nature Materials* **17**, 671 (2018).
- [39] G. Huang, H. Liu, H. Dong, and Z. He, Investigation of the clock transition and its pressure-dependent behavior of the trigonal  $^{171}\text{Yb}^{3+}$  centers in lithium niobate crystal, *Journal of Applied Physics* **133** (2023).
- [40] J. H. Davidson, P. J. Woodburn, A. D. Marsh, K. J. Olson, A. Olivera, A. Das, M. F. Askarani, W. Tittel,

- R. L. Cone, and C. W. Thiel, Measurement of the thulium ion spin hamiltonian in an yttrium gallium garnet host crystal, *Physical Review B* **104**, 134103 (2021).
- [41] C. Thiel, R. M. Macfarlane, Y. Sun, T. Böttger, N. Sinclair, W. Tittel, and R. Cone, Measuring and analyzing excitation-induced decoherence in rare-earth-doped optical materials, *Laser Physics* **24**, 106002 (2014).
- [42] R. Valivarthi, P. Umesh, C. John, K. A. Owen, V. B. Verma, S. W. Nam, D. Oblak, Q. Zhou, and W. Tittel, Measurement-device-independent quantum key distribution coexisting with classical communication, *Quantum Science and Technology* **4**, 045002 (2019).